Drill cuttings transport and deposition in complex annular geometries of deviated oil and gas wells: A multiphase flow analysis of positional variability

Drill cuttings transport and deposition in complex annular geometries of deviated oil and gas wells: A multiphase flow analysis of positional variability

Emmanuel I. Epelle and Dimitrios I. Gerogiorgis*

Institute for Materials and Processes (IMP), School of Engineering, University of Edinburgh, The Kings Buildings, Edinburgh, EH9 3FB, United kingdom

**Corresponding author: D.Gerogiorgis@ed.ac.uk (+441316517072)*

ABSTRACT

In this study, the two-fluid Eulerian-Eulerian multiphase flow model in ANSYS Fluent (v17.1) is adopted for the simulation of cuttings transport in a deviated annular geometry using two different non-Newtonian drilling fluids (described using the power law and Herschel- Bulkley models). The Syamlal-O'Brien interphase momentum exchange coefficient is implemented to capture non-spherical effects of the drill cuttings. The analysis conducted is based on the hypothesis that a position-dependent profile evaluation is expected to yield more insight into the transport process compared to a volume-averaged analysis over the entire flow domain. This is because the adopted simulation approach takes into account the microscopic particle properties which significantly affect the overall particle transport mechanism. However, this requires the application of robust postprocessing functionalities for data extraction from desired annular regions. Particle sizes considered are in the range of 0.002 m to 0.008 m with a sphericity range of 0.5 to 1.0. A rotational effect is incorporated in our model to describe the drillpipe motion in an annular wellbore with a vertical eccentricity of 0.6. The considered geometry contains a vertical, inclined and horizontal section with interconnecting upper and lower bends. The analysis of the particle velocity and concentration profiles revealed that the mud rheology, particle sphericity and particle sizes play vital roles in determining the cuttings removal process. It is particularly observed that the lower annular region of upper bend, is most susceptible to particle deposition with the lowest transport velocities observed. Our positional variability analysis has shown that the alternating dominance of nonspherical and spherical particles' velocities significantly depends on the nature of the flow (i.e. dense granular flow or dilute annular flow in the upper and lower sections respectively).

1. Introduction

Research efforts that address annular wellbore cleaning operations have continued to evolve over the years and this is because the resultant problems of inadequate hole cleaning can be highly detrimental to the overall economics and profitability of an oil and gas field. Some of these problems include premature drill bit wear, stuck drill pipe, poor formation data quality during logging operations (LWD), loss in operational time amongst many others. According to operation reports of Massie et al., (1995) and Hopkins and Leicksenring, (1995), a stuck drillpipe significantly contributed (70%) to the operational loss time experienced; a third of the stuck pipe problems were attributable to inadequate hole cleaning. Unfortunately, recent technological advancements in the drilling industry have also been accompanied with increased environmental complexity (especially during multilateral offshore drilling campaigns). Hence, it is expected that the contribution of wellbore cleaning problems to the overall loss in operational time is still significant.

As a result of the field-sensitive nature and the peculiarities of the challenges associated with in various practical drilling operations, generalising research findings can be tricky (Busch et al., 2018; Hakim et al., 2018; Yeu et al., 2019). However, some of the common unresolved questions that influence the decisions of all drilling engineers include: what mud viscosity should be used/what are the most favourable mud properties; what is the acceptable trade-off between the mud weight and its circulating velocity; how high should the fluid velocity be to avoid cuttings buildup; how does the annular clearance affect annular pressure drop (Epelle and Gerogiorgis, 2017; Katende et al., 2019). These decisions can be aided with the application of high-fidelity Computational Fluid Dynamics (CFD) models. Asides the numerical interpretation of results obtainable from CFD studies, enhanced particle transport visualisations is an extra functionality readily available in most CFD simulation tools. This further enhances the engineer's understanding and inevitably the performance improvement of the drilling operation.

Furthermore, the development of relevant and accurate cuttings transport models requires that experimental, modelling, and simulation studies target the respective flow scenarios obtainable in practical drilling operations. These flow scenarios include the geometrical, operational and environmental conditions that describe the industrial parameter space. However, it is impractical to solve the governing flow equations over typical wellbore lengths (several metres) in more than one dimension; this is due to very high computational time and resources required. Hence, the geometry involved here does not reflect the annular lengths obtainable in real operations, however, its structural characteristics and the operational parameters implemented conform to what is obtainable in practical deviated drilling operations; and is thus expected to provide some insights into the actual cuttings transport phenomena. In this work, we aim to provide answers to the earlier-posed questions by examining the impact of the non-Newtonian mud rheology and particle properties (size and sphericity) on particle velocity and concentrations profiles at different positions in the annulus.

2. Related Literature

Computational efforts (CFD-based) targeted at understanding the transport process of drill cuttings in an annular wellbore are numerous and can be generally grouped according to the modelling approach implemented (Eulerian-Eulerian, EE and the Lagrangian-Eulerian approach). It is also possible to categorize cuttings transport CFD studies based on the type of parameters considered/varied (Fluid circulation velocity, particle inlet velocity/ROP, particle size, particle sphericity, annular inclination, annular eccentricities, drill mud rheological properties etc.). This method of classification yield could become inconsistent considering the variety of parameters that can be varied and how intertwined their effects could be. Furthermore, another group of studies that implement DNS and LES models for annular fluid turbulence modelling exists (Chung et al., 2002; Feiz et al., 2003; Chung and Sung, 2005; Liu and Lu, 2005; Ninokata et al., 2006), but with very little consideration given to the treatment of the particulate phase; they however, pay detailed concentration to fluid shearing/viscous behaviour under different conditions. Hence, we limit the discussion to very recent pertinent research works in which the RANS equations are solved for the continuous and dispersed phases respectively.

Pang et al., (2018a) conducted a numerical study on cuttings transport behaviour using the Kinetic Theory of Granular flow using a power law non-Newtonian fluid. In their study, the swaying motion of

the cuttings due to drill pipe rotation was observed. They particularly observed that a critical rotational speed exists for which there is no additional contribution of drillpipe rotation to the cuttings transport phenomena. In another similar study of Pang et al., (2018b), a Herschel-Bulkley model was adopted for the rheological property description of the drilling mud. It was discovered that the flow behaviour index in the HB model is the most influential factor on the annular pressure drop computed. Sun et al., (2017) analysed the cuttings transport behaviour in a slimhole inclined annulus using a CFD-DEM model. They analysed the effects of annular fluid velocity, inclination angle, feed cuttings concentration and drill pipe rotation on the cuttings concentration. With the obtained results, they proposed a correlation for the critical cuttings deposition velocity in the annulus. The application of CFD-DEM models to three-phase multiphase flow description during unbalanced drilling with an aerated mud has been investigated by Akshik and Rajabi (2018). In their coupled approach, they implement the VOF model for capturing the gas-liquid interphase in the annulus. Several validation tests were performed and the obtained results showed good agreement with experimental results. They further observed that an increased gas injection rate causes a reduction in the cuttings volume fraction; hence the gas liquid ratio is an important factor that determines the wellbore cleaning efficiency. Also worth noting is that the impact of particle shape complexity has hardly been considered in cuttings transport studies. The studies of Al-Kayiem, (2010), Akhshik, et al., (2016), Mohammadzadeh et al., (2016) and Celigueta et al., (2016) address to varying degrees the effect of particle shape using the sphericity coefficient. Of all these studies, Akshik et al., (2016) pays detailed attention to the particle shape complexity using the CFD-DEM approach. It was thus necessary to also investigate shape complexity effects of cuttings using the Eulerian-Eulerian approach in this work.

Although non CFD-based, the work of Cayeaux et al. (2014), presented a new approach for monitoring annular cuttings deposition via a transient cuttings-transport model; this model incorporated closure laws for cuttings transport into a transient drill string model for the real time evaluation of wellbore cleaning conditions. Their model was calibrated against field data by parameter adjustment and provided real time monitoring of the drilling process. They were able to observe the positional annular velocity variation in different sections of the well; thus predicting regions prone to deposition. This positional variation is what we demonstrate in this work using CFD. The consideration of deviated wellbore geometry in most numerical studies is very scarce; however, Naganawa et al. 2017 proposed a 1D two-layer transient cuttings model for directional and extend-reach drilling applications. They validated their model against ECD field data obtained during LWD operations. For a more thorough review on the modelling of cuttings transport using CFD, the interested reader is referred to (Nazari et al; 2010; Kelin et al., 2013; Demiralp, 2014; Amanna et al., 2015; Epelle and Gerogiorgis, 2017; Manjula et al., 2017; Movreji et al, 207; Epelle and Gerogiorgis, 2018; Busch et al., 2018).

A major attribute of these studies that model annular cuttings transport is that several flow conditions are tested over a constant wellbore geometry or at best, with a variation in the angle of inclination of the wellbore. In these CFD studies, the variability in transport properties has only been accounted for along the wellbore's axial length and the radial direction in either wholly vertical, inclined or horizontal annuli. However, the impact of the annular geometries on the cuttings transport phenomena has been limited to scenarios in which the eccentricity (Epelle and Gerogiorgis, 2017; Heydari et al, 2017), wellbore-drillpipe diameter ratio (Ofei et al., 2014) and whirling drillpipe motion (Demiralp, 2014) are varied. These studies accounting for the annular geometrical complexities have shown its tremendous impact on the overall cuttings transport behaviour. To the best of our knowledge, the impact of geometrical changes (especially with some degree of deviation) on the transport phenomena has not been adequately studied. In this paper, we apply a physics-based multidimensional CFD approach for the elucidation of annular geometrical intricacies on the transport phenomena of drill cuttings. The work herein stems from the results of a previous analysis of ours that considers the effect of particle sphericity on cuttings transport (Epelle and Gerogiorgis, 2018b). The obtained results have been postprocessed in a different way (by extracting flow information from strategically positioned lines and planes in the annular domain, as well as considering threshold values) for better understanding of the cuttings transport phenomena. By adopting the positional variability analysis herein, we are able to numerically quantify in much greater detail (compared to our previous paper), the disparity between transport velocity and volume fraction between different particle shapes, but also offer a detailed visualisation in flow space. No previous study has evaluated the impact of particle shape on the degree of deposition

asymmetry (on either sides of a deviated annulus) at a microscopic level in different annular regions. This has been one of the foci of this study, which offers novel detailed results. Furthermore, our postprocessing method using cuttings concentration thresholds is new and has not been carried out in any previous study on cuttings transport, to the best of our knowledge. We expect this to hopefully establish a new trend for other researchers towards understanding their CFD results in depth.

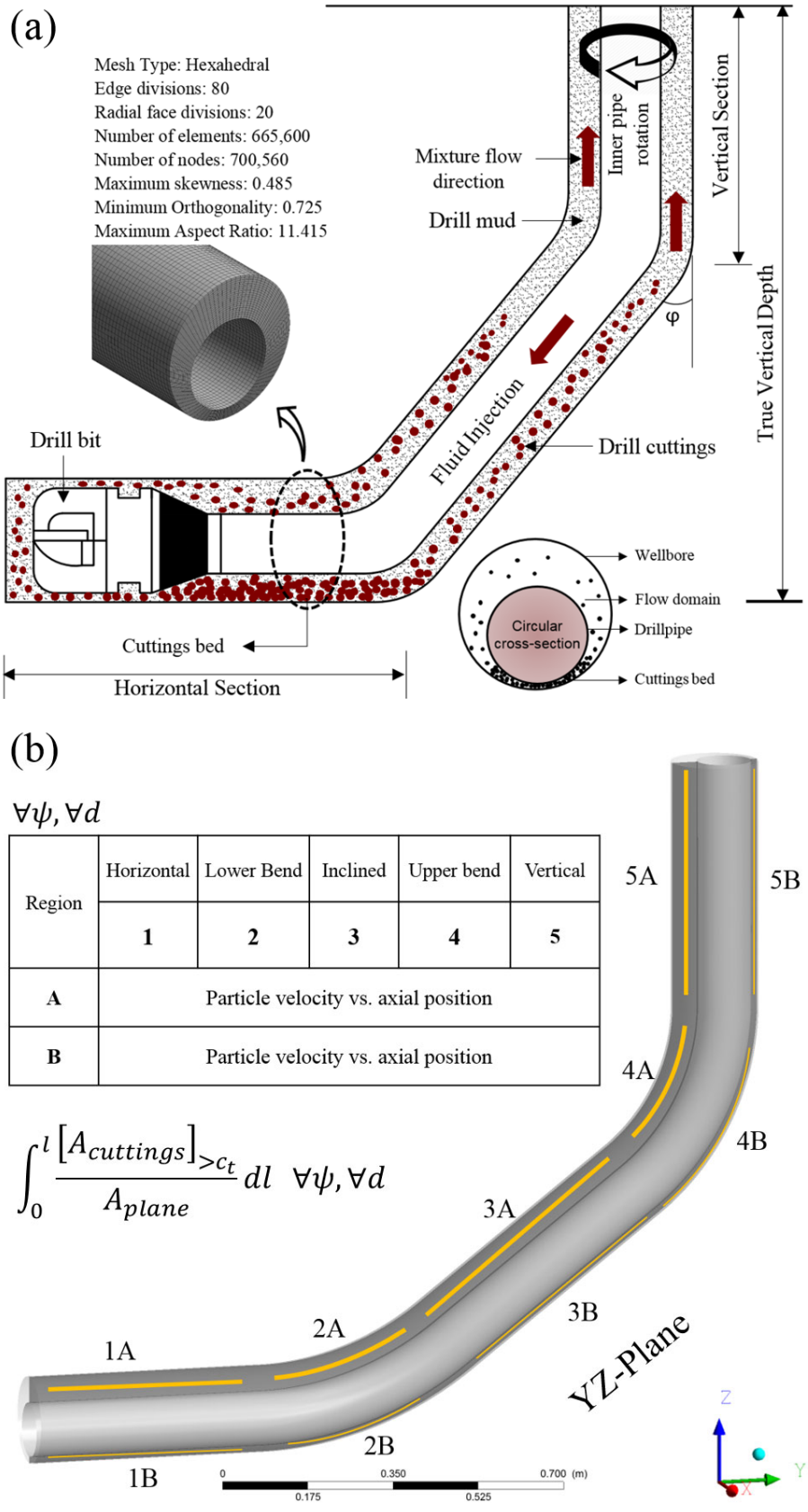

Figure 1. Wellbore geometry, meshing properties with sectional analyses planes and line segments.

3. Methodology

In this study, the two-fluid Eulerian-Eulerian approach is adopted for the simulation of the cuttings transport phenomena. Both phases (cuttings and drill mud) are actually separate phases but assumed as interpenetrating continua (Fluent, 2017). The governing equations include mass (Eq. 1) and momentum (Eqs. 2, 3) balances ensemble averaging for the respective phases. Phase interactions are incorporated to the EE model via the interphase momentum exchange coefficient (Syamlal and O'Brien, 1987; Eq. 4). Furthermore, particle sphericity (distinguishing spherical and non-spherical particles) is captured by the Wadell sphericity coefficient (ψ) and the related fluid-solid momentum exchange coefficient (K_{sl}, both in Eq. 4), using the Dalla-Valle drag coefficient (C_D) correlation (Eq. 5). The Wadell sphericity coefficient is the ratio of the surface area of an equivalent-volume sphere to the surface area of the actual non-spherical particle (Sobieski, 2009). The particle Reynolds number (Re_s), terminal velocity ($v_{r,s}$) and Syamlal-O'Brien model coefficients of the are defined in Eqs. 6-9, respectively.

Experimental studies of cuttings transport seldom account for particle shape irregularities, and this can be attributed to the inherent difficulty associated with accurate surface area measurement of irregular/non-spherical cuttings. In order to handle the insufficiencies of the continuum assumption of the solids cuttings phase, the Kinetic Theory of Granular Flow (KTGF) constitutive equations are applied to describe solid phase kinematic properties (Shah et al., 2015). A summary of these equations is presented in Table 1.

Particle concentration is key for calculating the effective fluid-particle suspension viscosity, which is affected by momentum exchange contributions due to both translation and collision. The respective granular viscosity terms due to kinetic (translational) motion (μ_s) and collisional particle interaction (λ_s) are described by Eqs. 10 and 11 respectively. Moreover, the collisional energy dissipation term within the solid phase due to inter-particle momentum exchange ($\gamma_{\Theta s}$) was derived by Lun et al. (1984) and is adopted in our CFD simulations (Eq. 12). For granular flow in the compressible regime (particle concentration is less than the maximum allowable value), a solids pressure can be calculated using Eq. 13 and included in the pressure gradient term of the solid phase momentum equation (Eq. 3) for improved accuracy.

A Maxwell particle velocity distribution is considered, with a granular temperature term is introduced into the solids pressure equation: this granular temperature of the solid phase (Θ_s) is proportional to the kinetic energy of the cuttings random annular motion and is given by Eq. 14. A correction factor ($g_{0,ss}$) which modifies the inter-particle collision probability in dense granular flow conditions (Eq. 15) is introduced into the Eulerian model; its physical significance can be thought of as the dimensionless distance between spherical particles. The application of the Johnson and Jackson (1987) friction pressure equation (Eq. 16) enables accurate prediction of frictional viscosity in dense granular flow conditions (when the particle concentration is near the packing limit).

Table 1: Principal and constitutive equations of the Eulerian-Eulerian model

Principal governing equations and hydrodynamic forces		
Continuity equation	$\frac{1}{\rho_{rs}}\left(\frac{\partial}{\partial t}(\alpha_s\rho_s) + \nabla\cdot(\alpha_s\rho_s\vec{v}_s) = \sum_{l=1}^{n}(\dot{m}_{ls} - \dot{m}_{sl})\right)$	(1)
Fluid-Fluid Momentum conservation equation	$\frac{\partial}{\partial t}(\alpha_l\rho_l\vec{v}_l) + \nabla\cdot(\alpha_l\rho_l\vec{v}_l\vec{v}_l) = -\alpha_l\nabla p + \nabla\cdot\bar{\bar{\tau}}_l + \alpha_l\rho_l\vec{g} + \sum_{s=1}^{N}[K_{ls}(\vec{v}_l - \vec{v}_s) + \dot{m}_{ls}\vec{v}_{ls} - \dot{m}_{sl}\vec{v}_{sl}] + (\vec{F}_q + \vec{F}_{lift,q} + \vec{F}_{wl,q} + \vec{F}_{vm,q} + \vec{F}_{td,q})$	(2)
Fluid-Solid Momentum conservation equation	$\frac{\partial}{\partial t}(\alpha_s\rho_s\vec{v}_s) + \nabla\cdot(\alpha_s\rho_s\vec{v}_s\vec{v}_s) = -\alpha_s\nabla p - \nabla p_s + \nabla\cdot\bar{\bar{\tau}}_s + \alpha_s\rho_s\vec{g} + \sum_{s=1}^{N}[K_{ls}(\vec{v}_l - \vec{v}_s) + \dot{m}_{ls}\vec{v}_{ls} - \dot{m}_{sl}\vec{v}_{sl}] + (\vec{F}_q + \vec{F}_{lift,q} + \vec{F}_{wl,q} + \vec{F}_{vm,q} + \vec{F}_{td,q})$	(3)
Fluid-solid exchange coefficient (Syamlal and O'Brien, 1987)	$K_{sl}' = \frac{3\alpha_s\alpha_l\rho_l}{4v_{r,s}^2\psi d_s}C_D\left(\frac{Re_s}{v_{r,s}}\right)\lvert\vec{v}_s - \vec{v}_l\rvert$	(4)

Drag coefficient (Dalla Valle, 1943)	$C_D = \left(0.63 + \frac{4.8}{\sqrt{\frac{Re_s}{v_{r,s}}}}\right)^2$	(5)
Particle Reynolds number	$Re_s = \frac{\rho_l d_s \lvert\vec{v}_s - \vec{v}_l\rvert}{\mu_l}$	(6)
Particle terminal velocity and coefficients	$v_{r,s} = 0.5\left(A - 0.06Re_s + \sqrt{(0.06Re_s)^2 + 0.12Re_s(2B - A) + A^2}\right)$	(7)
	$A = {\alpha_l}^{4.14}$	(8)
	$B = 0.8{\alpha_l}^{1.28}\ for\ \alpha_l \leq 0.85\ and\ B = 0.8{\alpha_l}^{2.65}\ for\ \alpha_l > 0.85$	(9)
Constitutive equations for solid-liquid multiphase flow		
Granular viscosity – Syamlal et al. 1993	$\mu_s = \frac{\alpha_s d_s \rho_S \sqrt{\Theta_S \pi}}{6(3 - e_{SS})}\left[1 + \frac{2}{5} g_{0,SS}\alpha_S(1 + e_{SS})(3e_{SS} - 1)\right]$	(10)
Granular bulk viscosity – Lun et al., 1984	$\lambda_S = \frac{4}{3}\alpha_S^2 \rho_S d_S g_{0,SS}(1 + e_{SS})\left[\frac{\Theta_S}{\pi}\right]^{1/2}$	(11)
Collisional dissipation of energy – Lun et al., 1984	$\gamma_{\Theta_S} = \frac{12(1 - e_{ss}^2)g_{0,SS}}{d_S\sqrt{\pi}}\rho_S \alpha_S^2 {\Theta_S}^{3/2}$	(12)
Solids Pressure – Lun et al., 1984	$p_s = \alpha_s \rho_S \Theta_S + 2\rho_S(1 + e_{SS})\alpha_S^2 g_{0,SS}\Theta_S$	(13)
Granular temperature	$\Theta_S = \frac{1}{3}\left(v_{S,i} \cdot v_{S,i}\right)$	(14)
Radial Distribution – Lun et al., 1984	$g_{0,SS} = \left[1 - \left(\frac{\alpha_s}{\alpha_{s,max}}\right)^{\frac{1}{3}}\right]^{-1}$	(15)
Frictional Pressure – Johnson and Jackson, 1987	$P_{friction} = Fr\frac{(\alpha_s - \alpha_{s,\min})^n}{(\alpha_{s,max} - \alpha_s)^p}$	(16)

Earlier industrially adopted correlations, e.g. those by Hopkins (1967) and Larsen (1997) allow for quick determination of cuttings slip velocity and Critical Transport Fluid Velocity, *CTVF* (Eqs. 17-21); where *CTV* is the cuttings transport velocity, *ESV* is the estimated slip velocity, μ_a is the apparent and μ_p is the plastic viscosity. However, with increasingly difficult-to-drill environments and highly complex multiphase flow scenarios, such empirical methods break down because of their limited extent of applicability. Therefore, numerical-based CFD methods (described here) gain overwhelming acceptance in industry compared to these empirical correlations and simplistic single-phase analytical models (such as the Hagen-Poiseuille equation/Eq. 22, which can only capture incompressible Newtonian laminar flow and thus cannot credibly handle real-world drilling systems).

$$CTFV = CTV + ESV \tag{17}$$

$$CTV = \frac{1}{\left[1 - \left(\frac{D_{pipe}}{D_{wb}}\right)^2\right]\left(0.64 + \frac{18.16}{ROP}\right)} \tag{18}$$

$$ESV = 0.00516\mu_a + 3.006\ for\ \mu_a < 53cP \tag{19}$$

$$ESV = 0.02554(\mu_a - 53) + 3.28\ for\ \mu_a > 53cP \tag{20}$$

$$\mu_a = \mu_a + \frac{5Y_p(D_{hole} - D_{pipe})}{CFTV} \tag{21}$$

$$Q = -\frac{dP}{dx}\frac{\pi}{\mu}\left[R_2^4 - R_1^4 - \frac{(R_2^2 - R_1^2)^2}{\ln\left(\frac{R_2}{R_1}\right)}\right] \tag{22}$$

3.1 Geometrical, fluid and particle properties

The annular flow geometry and the type of meshing adopted are illustrated in Fig. 1. Table 2 also shows the dimensions of the geometry, the fluid and particle properties as well as simulation set up parameters/boundary conditions. The rheological description of two separate drilling muds were implemented in the simulation and the resulting cuttings velocity and concentration profiles are comparatively assessed. It was also essential to evaluate the optimum number of meshing elements for which numerical solutions obtained are grid independent. In this study, it was discovered that 665,600 elements were required.

3.2 Simulation set up and computations

Numerical solutions of the flow field were obtained by applying Fluent's pressure-based solver to the RANS equations using the finite volume discretisation method. The phase-coupled SIMPLE scheme was adopted for pressure-velocity coupling and the spatial discretization was carried out using the QUICK method (robust for hexahedral meshing methods). The transient flow behaviour was simulated using a time step of $5 \cdot 10^{-4}$ and the convergence criterion for all equations solved was set as (10^{-4}) at each time step. The simulation was run for a total period of 5 seconds using The University of Edinburgh's high performance computing facility (Eddie mark 3 – Scientific Linux 7 Operating System) with 32 cores (2.4 GHz Inter ® - Xenon ® processor) and 64 GB of RAM.

Table 2. Simulation input parameters

	Drilling Mud 1	**Drilling Mud 2**
Geometry		
Drill pipe diameter, d_{pipe} (m)	0.113	0.113
Wellbore diameter, d_{wb} (m)	0.180	0.180
Computational length, L (m)	2.340	2.340
Fluid properties		
Composition	0.5% CMC Solution	0.5% CMC + 4% Bentonite
Density, ρ_l (kg.m^{-3})	1000	1030
Yield stress, τ_0 (Pa)	0	46.5
Consistency index, K (Pa.s^n)	0.5239	0.6482
Flow behaviour index, n	0.60	0.7
Particle properties		
Cuttings diameter, d_s (m)	0.002, 0.003, 0.004, 0.005, and 0.008	0.002, 0.003, 0.004, 0.005, and 0.008
Cuttings density, ρ_s (kg.m^{-3})	2800	2800
Sphericity, ψ	0.50, 0.75, 1.00	0.50, 0.75, 1.00
Drilling variables		
Fluid circulation velocity, v_l (m.s^{-1})	0.8	0.8
Cuttings inlet velocity, v_s (m.s^{-1})	0.5	0.5
Drill pipe rotation, Ω (rpm)	100	100
Hole eccentricity, e	0.6	0.6

4. Results and Discussion

4.1 Model validation and sectional analyses

The described methodology is applied to the experimental measurements of pressure drop and cuttings concentration (Duan et al., 2006; Sorgun, 2010). Validation results are shown in Fig. 3 of Epelle and Gerogiorgis, (2018c). Our CFD model is able to reproduce the experimental data within an error range of 11%; thus substantiating the validity of the adopted modelling methodology. The sectional analysis methods for the annular cuttings concentration and velocity are presented next. This is expected to provide physical details of the actual behavior of the cuttings at different regions in the annulus. The circular plane in Fig. 1a is positioned such that the transport behavior in the horizontal, inclined, vertical and transition (lower and upper bend) regions are captured (Figs. 6a, 7a, 8a, 9a). Furthermore, line segments are constructed along the YZ plane (Fig. 1b), which symmetrically divides the annulus into front and back halves. Because the present study builds upon our recent publication which specifically addressed and visualised pressure drop profiles (Epelle and Gerogiorgis, 2018b), we have decided to only focus on the positional variation of cuttings velocity and concentration (the main novel elements here).

4.2 Line segment analysis of cuttings velocity profiles in the annulus using drilling mud 1

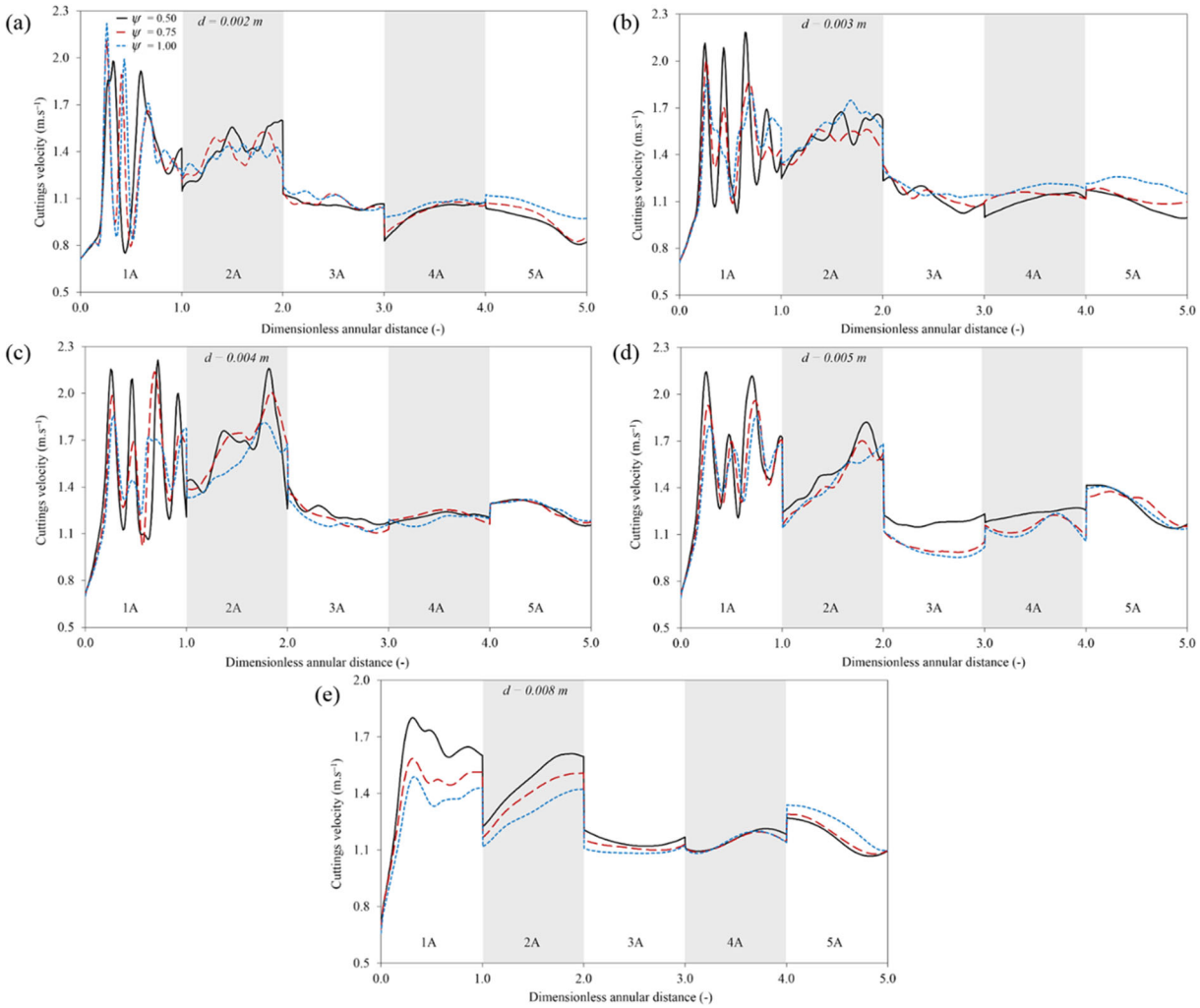

Figure 2: Cuttings velocity profiles in the line segments of the wider annular region "A" using drilling mud 1.

It can be observed that all particles within the sphericity range considered demonstrated significant velocity fluctuations at the entrance (Regions 1A and 1B) of the flow domain (Figs. 2 and 3). As the particles move further into the annulus, the frequency of the velocity fluctuations reduces and the velocity profiles depicted become more tractable. The profiles in Region 1A thus indicate the presence of turbulence whose effect reduces as the particles travel further into the annulus due to the inevitable drop in pressure. It is generally noticed that an abrupt drop in velocity ensues as the particles enter the inclined sections (Region 3A, Figs. 2 and 3) of the annulus, which is 40° from the horizontal. This observation is similar to that of Pang et al. 2018a in which they discovered that well inclination around 35° – 65° were the most difficult cuttings transport conditions. The occurrence of this abrupt velocity reduction is particularly intensified at the narrower annular sections (Region B) as shown in Fig. 3. Also observed is the lower cuttings velocities in the lower Region B compared to the upper Region A. The eccentric configuration of the domain favors the flow of cuttings in the wider region where spatial flow resistance (due to the boundaries) is least.

As the particles travel up the annulus, it is noticed that the highest flow velocities are dependent on the particle size and sphericity. In Region A – Fig. 2a & b, (for $d = 0.002$ m and $d = 0.003$ m), it is difficult to tell which of the particles (highly nonspherical, $\psi = 0.50$, moderately nonspherical, $\psi = 0.75$, or the perfectly spherical particles, $\psi = 1.00$), consistently has the highest velocity. This alternating dominance in travel velocity displayed by these smaller particles is highly location dependent (1A, 2A, 3A, 4A & 5A). However, with the increase in particle size ($d = 0.004$ m, 0.005 m, & 0.008 m), it becomes clearer that the highly nonspherical particles tend to dominate the velocities of the other particles ($\psi = 0.75$, 1.00). Furthermore, as the particles get bigger, the difference in the velocity profiles of the considered sphericities, gets larger particularly for the 0.005 m and 0.008 m particles (Fig. 2e and 2e). This finding

compares favorably with experiential findings, which reveal that nonspherical particles interact more with the fluid by engaging in secondary motion about the particles' axis (Yow et al, 2005; Mando et al. 2007; Byron et al. 2015). This in turn yields a better response of nonspherical particles to the fluid motion compared to spherical particles, which do not engage in this kind of motion and hence tend to fall through the fluid more easily.

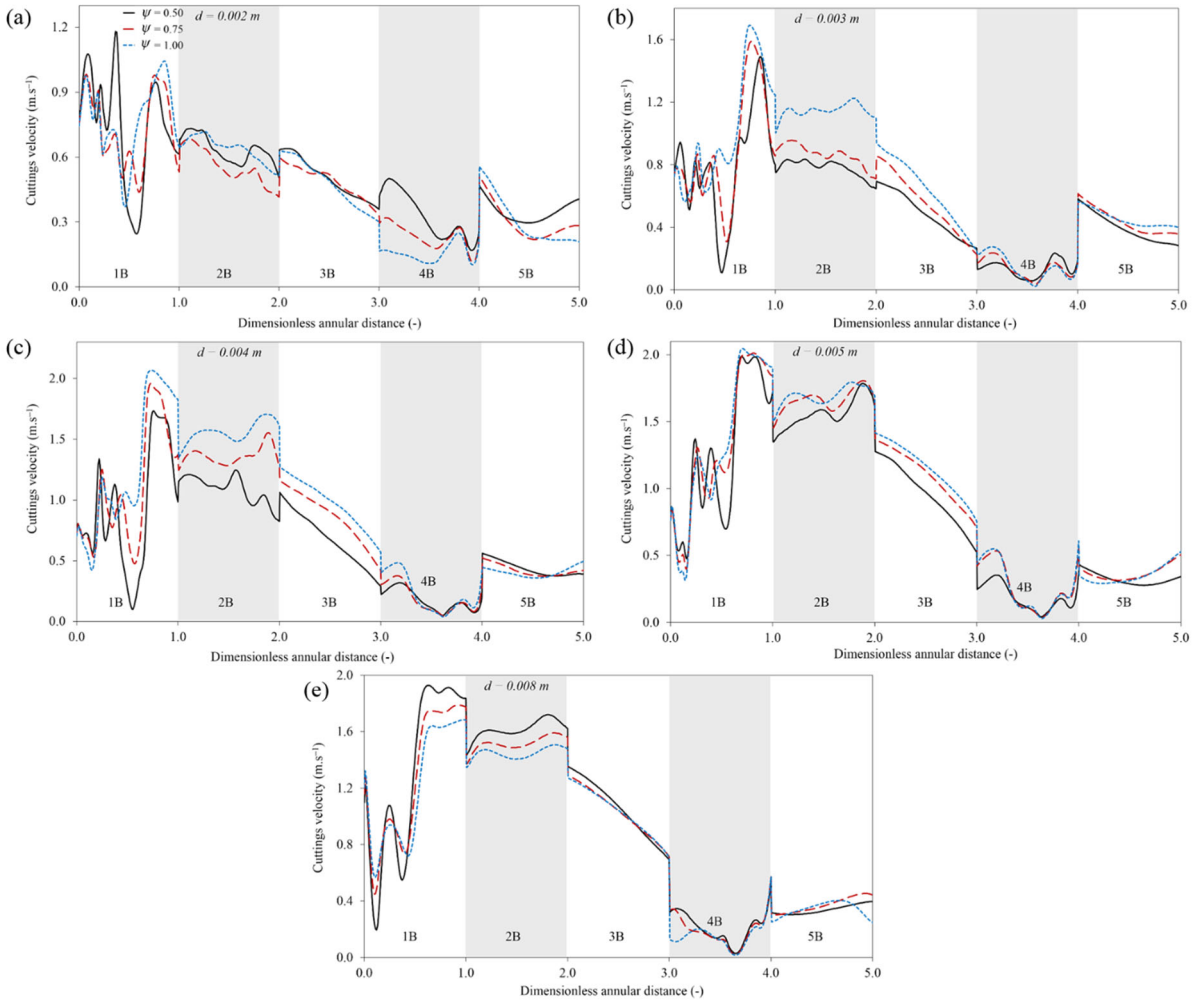

Figure 3: Cuttings velocity profiles in the line segments of the narrower annular region "B" using drilling mud 1.

It is also observed (Fig. 3a-d) that the perfectly spherical particles tend to have the highest velocities at most line segments in the lower/narrower annular region (Region B). This effect is significant in the inclined regions. This occurrence demonstrates the strong disparity between dilute granular flow in the wider section (lower particle concentration relative to the fluid – Region A) and dense granular flow (high particle concentration relative to the fluid – Region B). We attribute this effect to the lower particle drag spherical particles due to their tendency to engage in rolling motion; this kind of motion is hardly possible for nonspherical particles, which naturally engage in sliding motion under a densely concentrated/packed flow scenario. Furthermore, the packing behavior of spherical particles allows extra fluid interaction with the particles (which increases particle velocity) due to larger void spaces created, compared to a tighter packing (reduced void spaces) that is attainable with non-spherical particles. However, in Fig. 3e, for the largest particles (d = 0.008 m), it is noticed that the highly non-spherical particles dominate the group velocity profile. This is contrary to what is observed in Fig. 3a-d. We attribute this phenomena to the highly skewed (shifted to one side of the YZ Plane) deposition pattern of the largest particles (0.008 m) compared to other smaller particles (0.002 – 0.003 m), so that the line segments (Regions 1B – 3B) pass through annular locations exposed to dilute granular flow conditions as in Region A; hence nonspherical particles still possess the highest travel velocities in Fig. 3e. This shifted deposition pattern will be further discussed in the analysis of the cuttings deposition patterns across the sectional planes. Although the EE model adopted here is unable to fully resolve/directly capture the kinematics of particle rolling (spherical) and sliding (nonspherical) motion,

it is observed that pertinent geometry-related flow attributes of these particles illustrated in the simulation results, conform to their actual physical behavior.

4.3 Line segment analysis of cuttings velocity profiles in the annulus using drilling mud 2

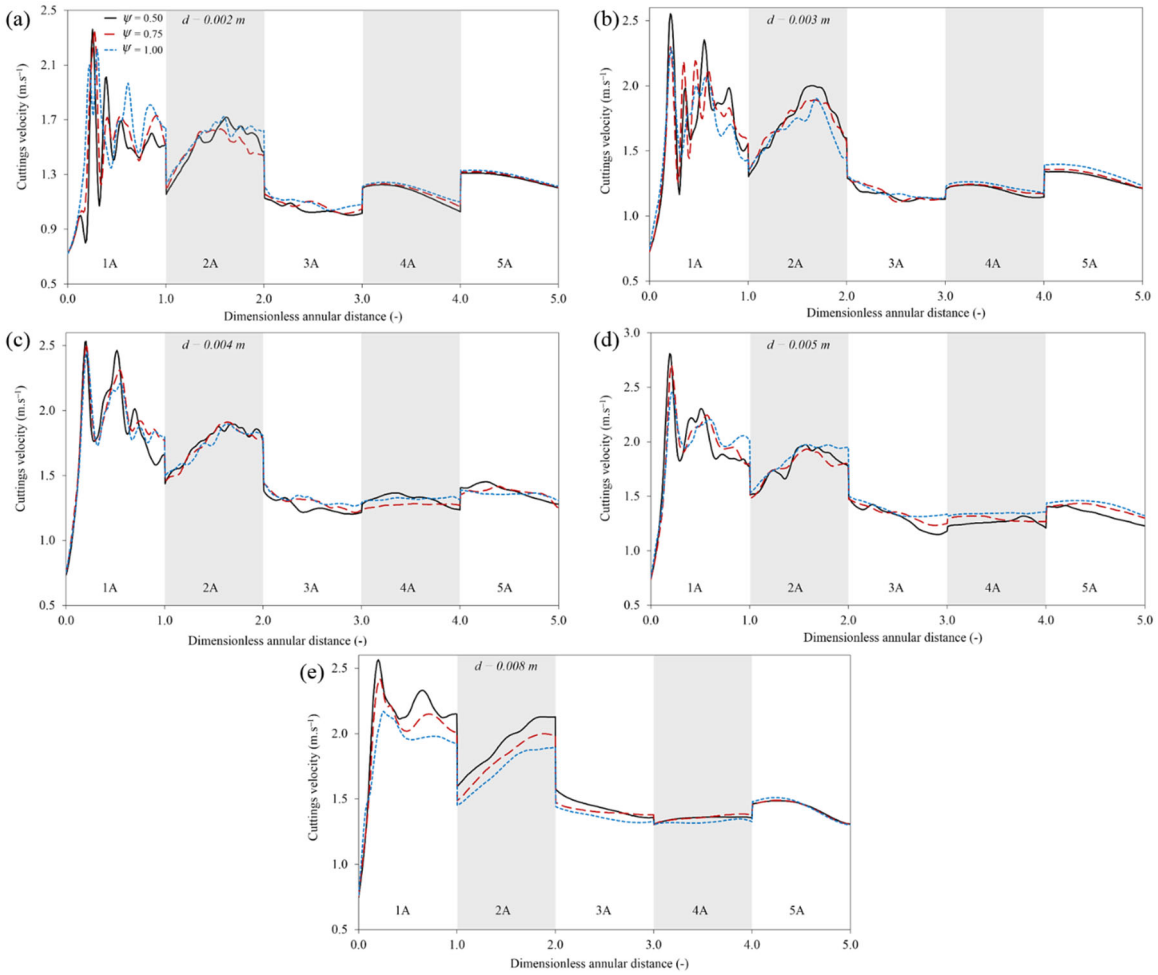

Figure 4: Cuttings velocity profiles in the line segments of the wider annular region "A" using drilling mud 2.

Very similar observation to those of drilling mud 1 are made in the case of drilling mud 2. However, some subtle differences exist which are discussed. Compared to the first drilling mud, for each particle size (Fig. 2), there is minimal disparity between the velocity profiles for the particles of different sphericities (Fig. 4) when the second drilling mud is used. The viscosity enhancement of drilling mud 2 thus reduces the velocity disparities initially noticed with the CMC fluid for the different particle shapes. The difference in the velocity profiles however, only gets clearer with the largest particle size (Fig. 4e). Again, we notice the highly nonspherical particle having the highest velocity.

In the lower annular sections (Region B, Fig. 5), it is particularly observed that for all particle sizes, the different particle shapes experience very similar transport velocity as they enter the upper bend and vertical regions respectively (Regions 4B and 5B). This implies that the complexities of particle shape significantly affect the transport process in the horizontal and inclined regions respectively compared to the vertical regions. For all cases considered (including drilling mud 1), the particles experience the lowest transport velocities in Region 4B; this is the region that is most susceptible to particle deposition and will be further discussed in Sections 4.4 and 4.5 respectively.

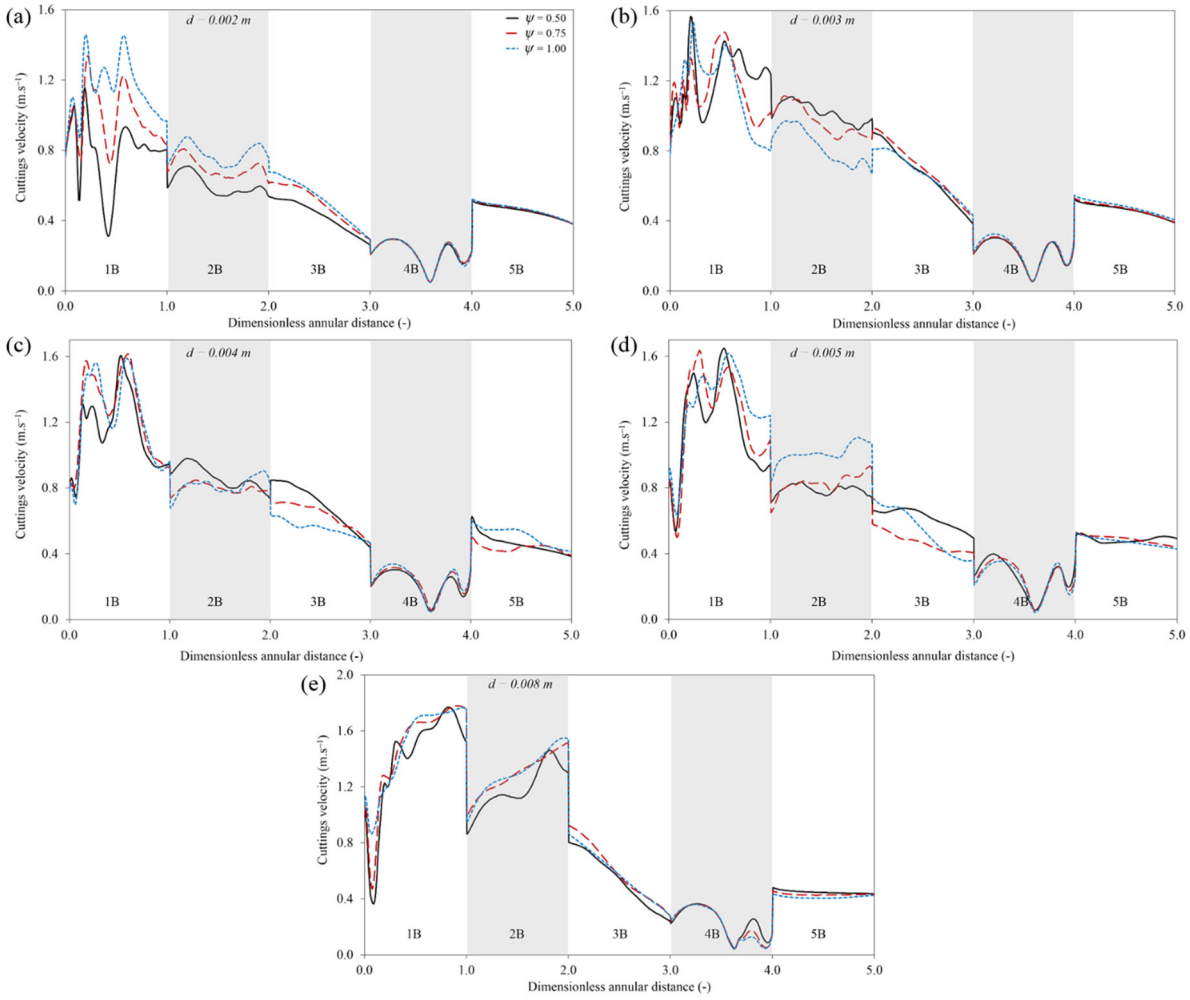

Figure 5: Cuttings velocity profiles in the line segments of the narrower annular region "B" using drilling mud 2.

It is well established that nonspherical particles generally travel faster when transported in an annulus (as demonstrated in volume-averaged analysis of **MS1** and experiments of Byron, 2015). The results presented herein (based on a regional postprocessing analysis) reveal that this is not necessarily the case in all annular regions. Our positional variability analysis shows this variable dominance of nonspherical and spherical particle velocities significantly depends on the nature of the flow and the annular region considered (i.e. dense granular flow or dilute annular flow in the upper and lower sections respectively).

Furthermore, the rather mild impact of cuttings sphericity on the travel velocity reflected in the volume-averaged results (of **MS1**) is seen to only manifest in certain regions of the annulus in this work. This study shows this disparity is larger in other regions (esp. 1 and 2), demonstrating the inherent transport differences of all particle shapes considered. These observations are similar but different to those obtained in our cuttings concentration analyses published in advance of this paper.

4.4 Sectional analysis of cuttings deposition in the annulus using drilling mud 1

As demonstrated in Fig. 6a, seven equidistant perpendicular cross sections of the annular geometry are used to further gain insight into the cuttings transport phenomena. The area fraction of the cuttings bed across the different planes is found using the expression in Fig 6a. Thresholds of cuttings concentration (c_t = 0.4 and 0.5) are respectively applied over the averaged volume fraction in the flow domain, before evaluating the expression. A similar procedure is adopted to analyse cuttings deposition along a symmetric YZ plane (Fig. 1b). The results are systematically grouped to analyse the impacts of particle sphericity and diameter coherently.

As expected, there is a general reduction in the cuttings deposition area as the cuttings concentration threshold increases. A consistent peak in cuttings concentration is also noticed on plane 5 (Fig. 6). This is in accordance with the earlier explained intense deposition at the upper annular bend (Region 4B;

Figs. 2-5). More importantly, increased variability of the cuttings concentration with respect to sphericity is noticed in all cases compared to the volume-averaged analysis in (Epelle and Gerogiorgis, 2018). For a threshold of 0.4 and a particle diameter of 0.008 m (Fig. 6i), we observe two peaks in the concentration profile, which correspond to the upper and lower bend respectively. The plots shown with respect to the particle diameters (Figs. 6b-d) reveal that the 0.008 m particles often peak in concentration at the sixth plane compared to other diameters with peaks at plane 5 (Figs. 6b-d; Figs. 7b-d).

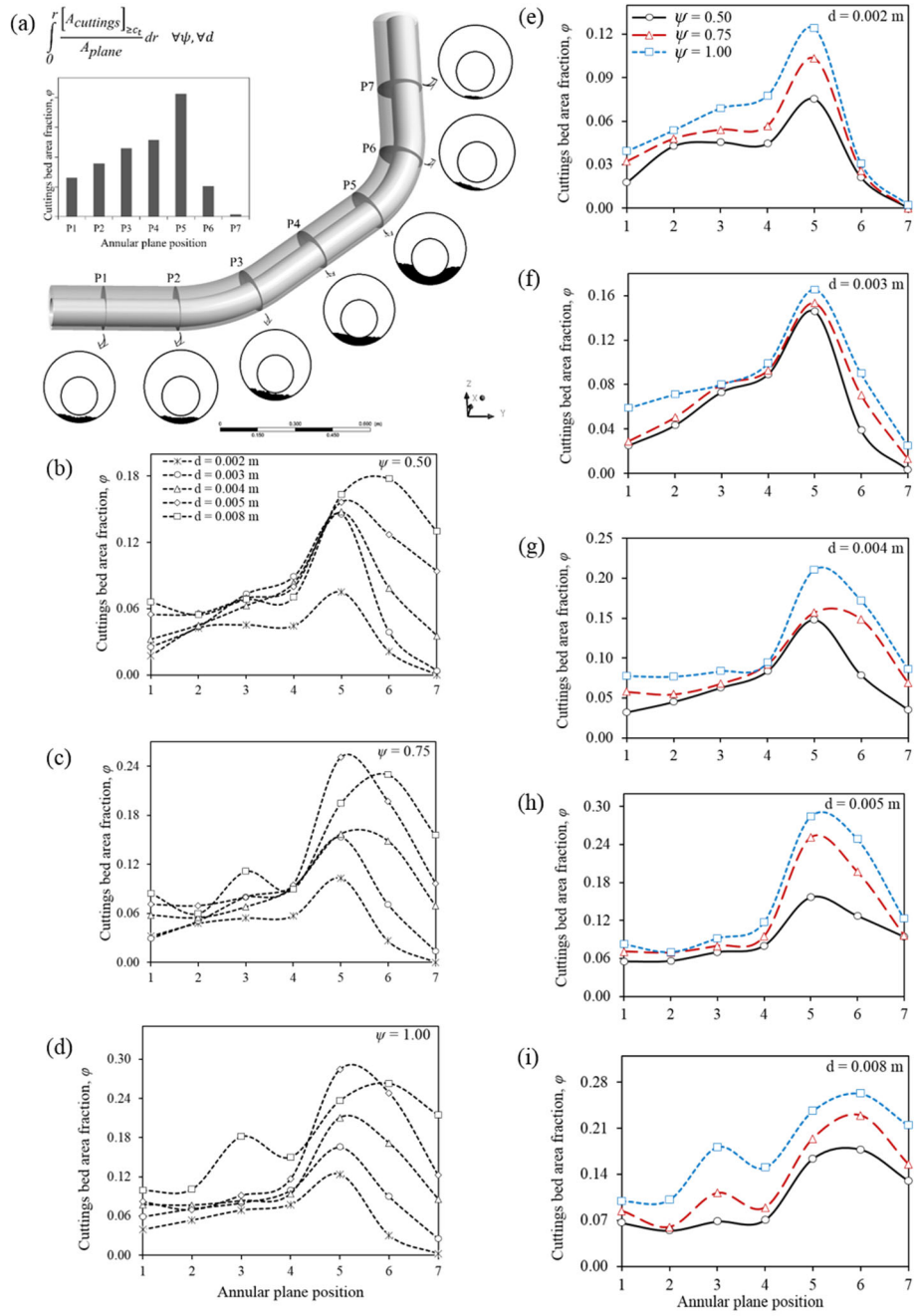

Figure 6. Analysis of particle concentration along the annulus, using a cuttings concentration threshold of $\varphi = 0.4$ and the CMC drilling mud 1

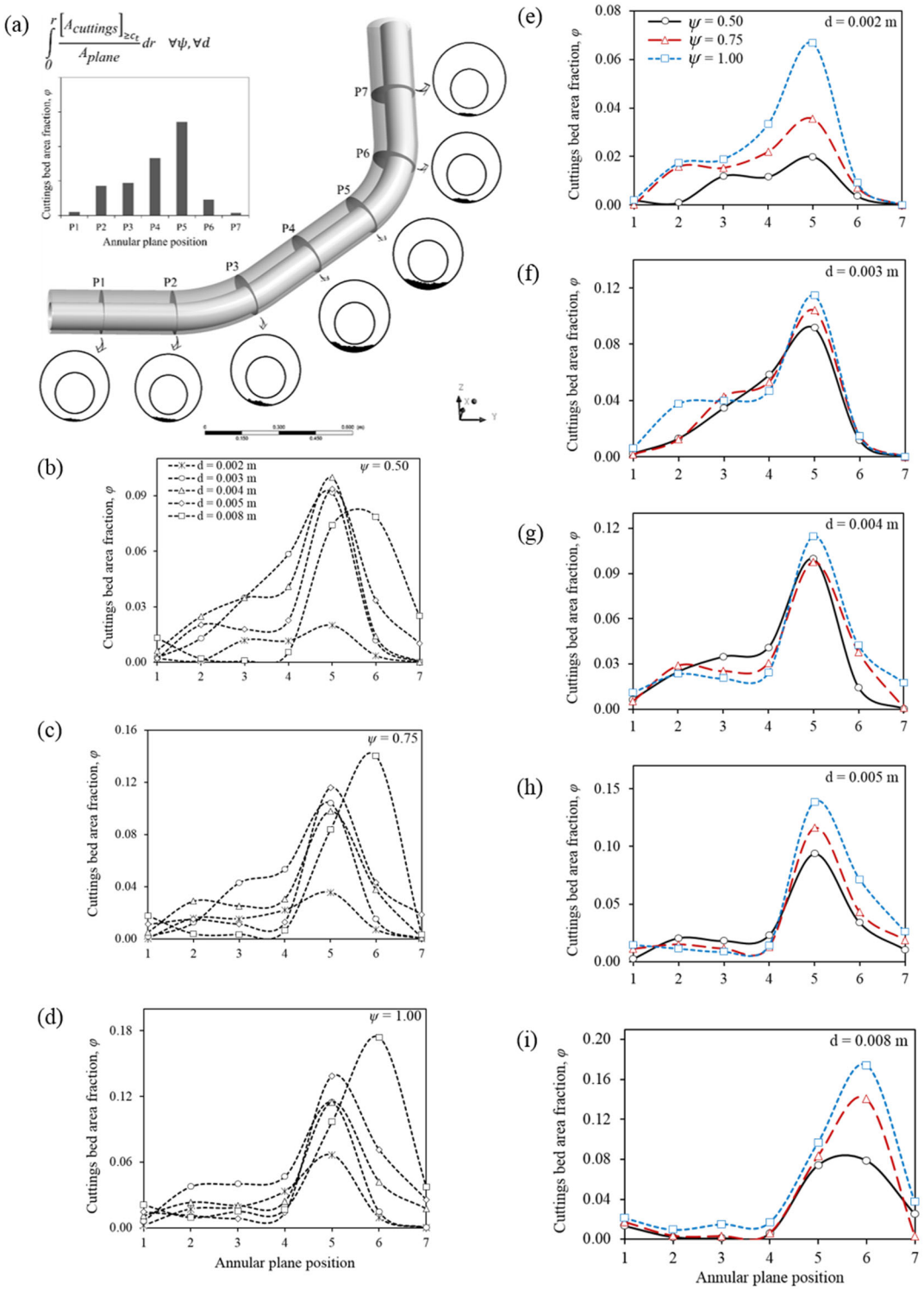

Figure 7. Analysis of particle concentration along the annulus, using a cuttings concentration threshold of $\varphi = 0.5$ and the CMC drilling mud 1.

4.5 Sectional analysis of cuttings deposition in the annulus using drilling mud 2

Similar analysis to that applied using mud 1 is also utilized here. Figs. 8 and 9 illustrate the peculiarities of the cuttings deposition pattern observed as a function of particle sphericity and diameter using the superior drilling fluid.

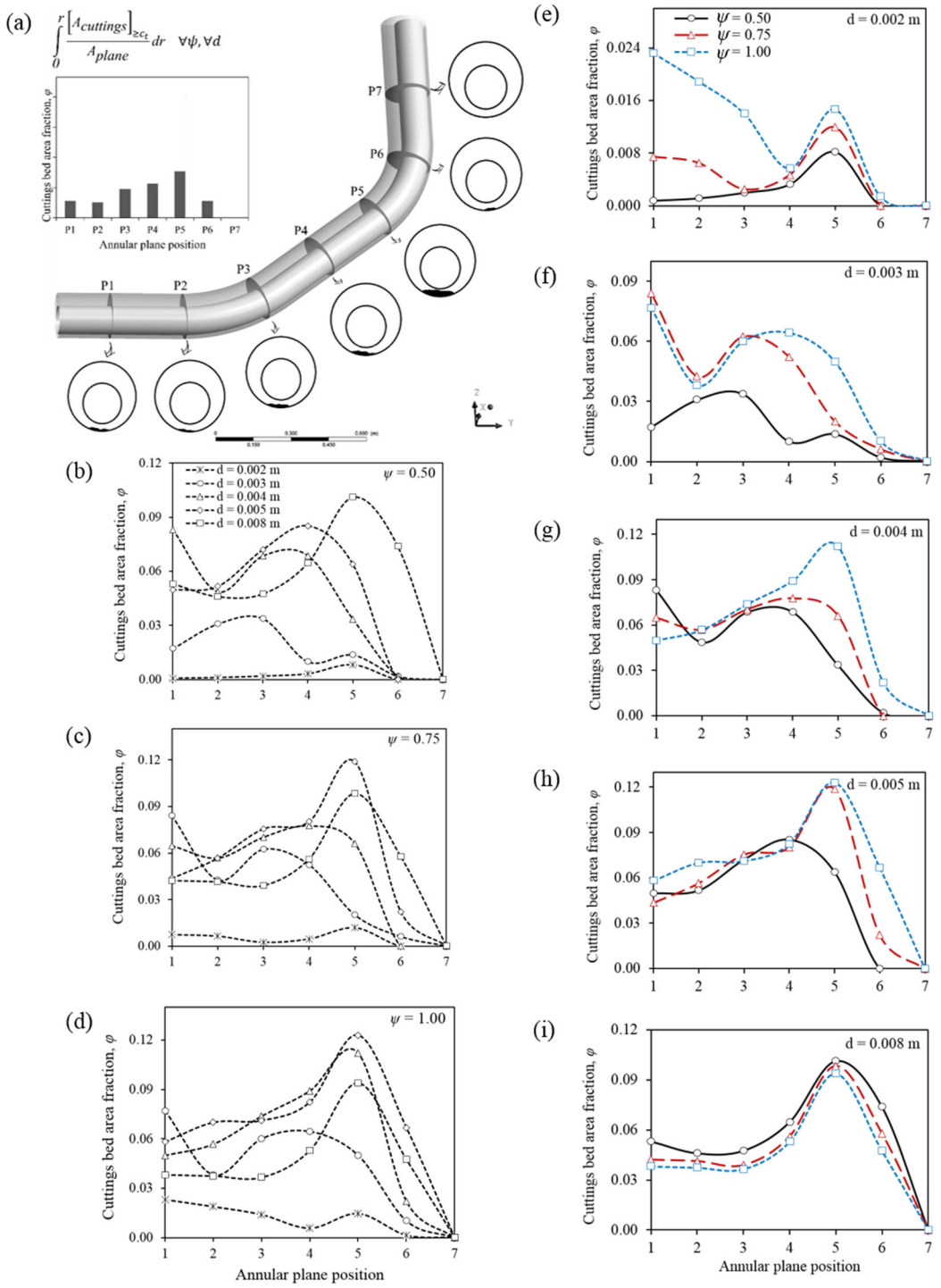

Figure 8. Analysis of particle concentration along the annulus, using a cuttings concentration threshold of $\varphi = 0.4$ and the CMC + Bentonite drilling mud 2.

It is generally observed that stronger deposition in the horizontal section (planes 1 and 2; Figs. 8e-f) occurs over time with the second drilling mud compared to the deposition pattern observed for other particle diameters (Figs. 8g-i). In addition, there is a reversal in deposition intensity by the 0.008 m cuttings, in the sectional analysis performed herein. This phenomenon may be attributed to the reduced cross sectional area (due to increased deposition of the non-spherical particles) which translates to an increased averaged velocity especially in the dilute flow regions (Region A). The second drilling mud (Figs. 8 and 9) reveals no deposition in planes 6 and 7 due to the near-vertical alignment of the geometry and its superior performance.

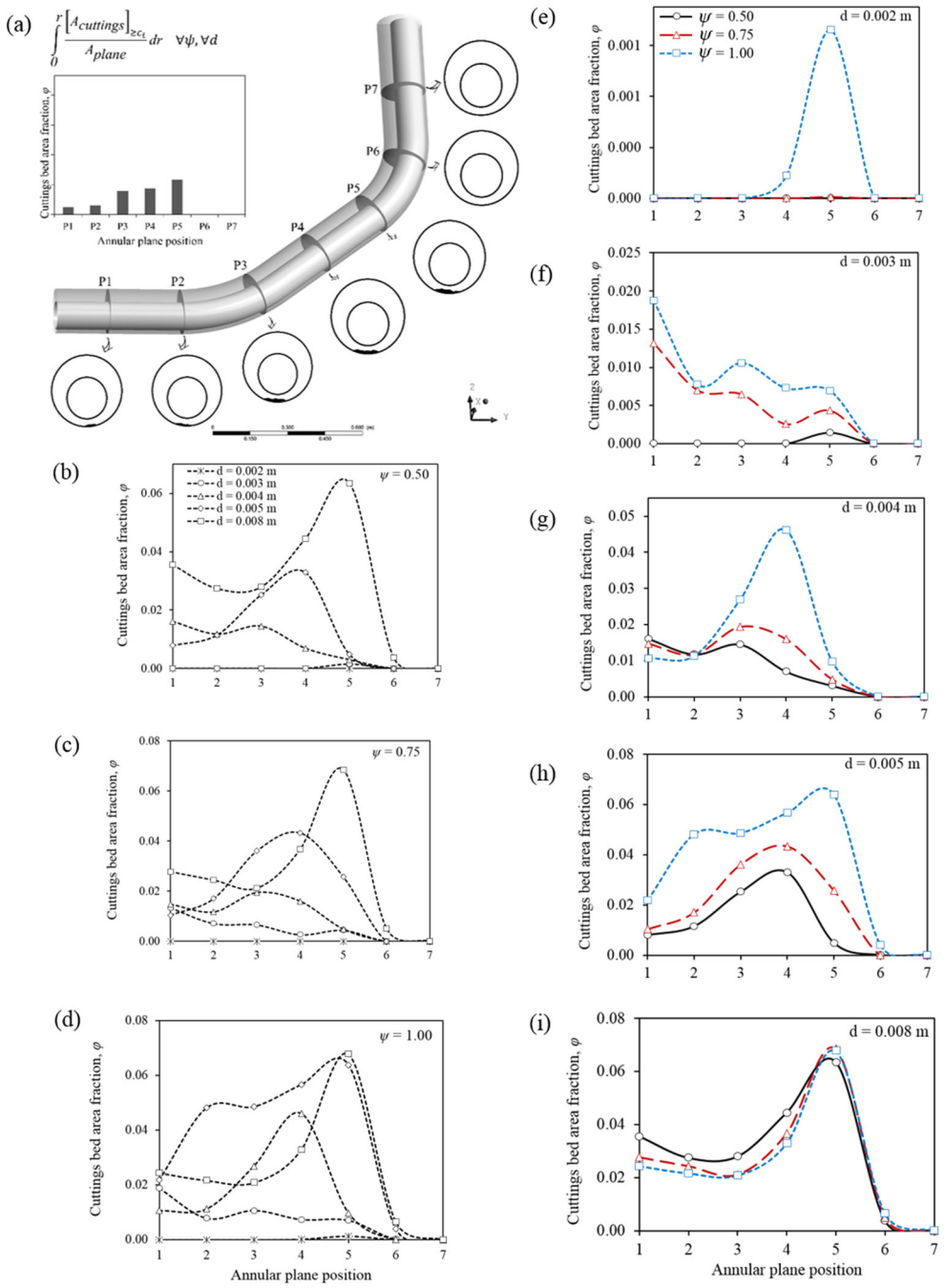

Figure 9. Analysis of particle concentration along the annulus, using a cuttings concentration threshold of $\varphi = 0.5$ and the CMC + Bentonite drilling mud 2.

Since the YZ plane in Fig. 1b divides the annulus into two equal halves along the flow direction, it is possible to ascertain the impact of particle sphericity and diameter on the symmetry of the deposition pattern. When the first drilling mud is used, it is observed that the cuttings concentration decreases as the diameter increases for a threshold of 0.4 and 0.5 respectively (Fig. 10). This explains the increased asymmetry (shifted deposition to one side of the annulus – non-centralised along the YZ plane) caused by larger particles as discussed in detail by Epelle and Gerogiorgis, 2018. This shifted deposition pattern can be attributed to the effect of drillpipe rotational/swaying motion on the particles and also because the increase in particle size makes it difficult for the particles to fit in a compacted manner in the narrower annular region (B). Thus, intense and centralised particle deposition that can be captured by the YZ plane (Fig. 1b) for the smaller-sized particles is often not shown by the same plane for the larger sized particles. This phenomenon is reflected in the velocity profiles in Fig. 3e and discussed in section 4.2.

The second drilling which is able to maintain uniform positional displacement of drill cuttings as a result of its superior viscosity characteristics and shows a different profile. While the smaller particles

(0.002 m) are readily carried with little or no deposition (Figs. 10c and 10d), larger particles yield an increased deposition along the YZ plane until a slight reduction ensues from a diameter of 0.005 m. This observed pattern compared to Figs. 10a and 10b; is indicative of the rather centralised deposition pattern, which the cuttings of various sizes experience with the second drilling mud. Thus, the strongly shifted deposition pattern observed with drilling mud 1 is not the case with drilling mud 2. While the 0.4 and 0.5 thresholds are generally representative of the holistic transport behaviour of the densely concentrated regions, the profiles of the 0.6 threshold (not shown herein) were severely affected by the inherent stochasticity of the transient transport process. Furthermore, the simulation settings of CFD solver (Fluent 17.1) ensures that the solids packing density is limited to a value of 0.63. This allows for some void space (occupied by the liquid) between the particles so that there is minimal momentum transfer from the drilling mud to the particles. As the applied cuttings concentration threshold approaches this value (0.63), it is likely that the uncertainty in the transient statistical averaging of the cuttings concentration becomes more significant. Accounting for this uncertainty is a subject of future investigations.

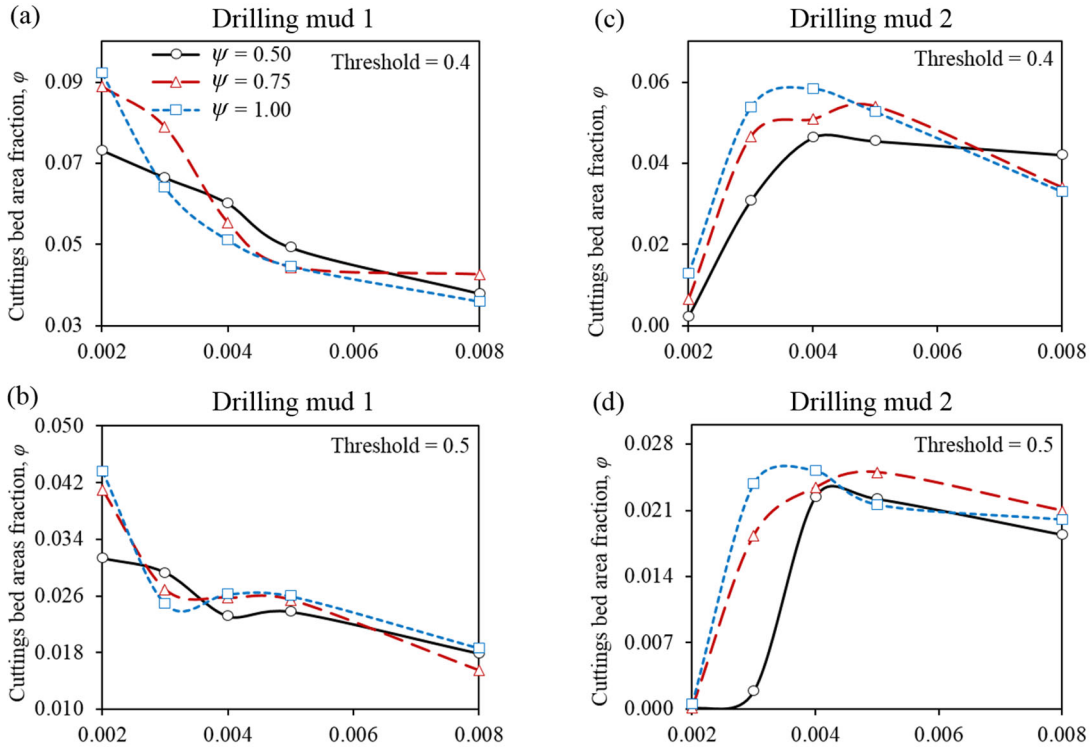

Figure 10. Analysis of particle concentration along the YZ symmetrical plane in the annulus, using a cuttings concentration threshold of $\varphi = 0.4$ and $\varphi = 0.5$ for both drilling muds.

5. Conclusions

This paper presents a transient analysis of drill cuttings transport behaviour in a deviated annulus using the Eulerian-Eulerian model in Ansys Fluent. Principally demonstrated in this work is the application of several line segments and cutting planes for the elucidation of the position-dependent cuttings transport behaviour in the annulus. We draw the following conclusions from the observations made.

- Despite the fact that CFD simulations carried out here only consider a mono-dispersed particle distribution (both in terms of size and shape), the presented profiles indicate that flow complexity will further increase due to polydispersity and its multiple momentum transfer mechanisms (particle-fluid and particle-particle interactions). CFD studies accounting for polydisperse cuttings distribution are scarce (if any), implying great opportunities.

- Although the velocity analyses here are carried out along lines, a holistic picture of the transport velocities' dependence on particle shape is attainable via a volume-averaged analysis over the entire multifaceted domain. Just as the overall macroscopic phenomena over the entire flow

domain is often desired, analysis via enhanced spatial resolution that yields the cuttings transport behavior at a more refined level cannot be neglected.

- Sectional analysis of cuttings deposition along several planes in the annulus provided better variability in cuttings concentration as a function of particle sphericity compared to the volume-averaged analysis.
- The sectional analysis of the deposition profiles has shown that the narrower region of the upper annular bend is most likely to retain the highest amount of drill cuttings.
- Neglecting particle shape effects could result in severe underestimation of the required velocity and thus the pressure drop necessary for a deposition-free transport scenario.
- Spatial velocity variation in the annulus shows that the wider annular sections are more readily experience dilute flow of cuttings (due to high velocity of travel) compared to the lower annular regions where dense granular flow is prominent.
- The particle shape with the dominant velocity depends on the annular location and the nature of the flow (dilute or dense). Nonspherical particles tend to dominate the group velocity profiles in the dilute granular flow region (A), whereas, spherical particles have the highest velocities in the dense granular regions (B).
- The results presented herein (based on a regional postprocessing analysis) reveal that the velocity of non-spherical particles are not necessarily higher than those of spherical particles in all annular regions. Our positional variability analysis has shown that the variable dominance of nonspherical and spherical particles' velocities significantly depends on the nature of the flow (i.e. dense granular flow or dilute annular flow in the upper and lower sections respectively).

6. Acknowledgements

The authors gratefully acknowledge the financial support of the University of Edinburgh via a PhD scholarship awarded to Mr E. I. Epelle. Moreover, Dr D. I. Gerogiorgis acknowledges a Royal Academy of Engineering (RAEng) Industrial Fellowship. Tabulated and cited literature data suffice for reproduction of all original CFD simulation results and no other supporting data are required to ensure reproducibility.

7. Nomenclature and Acronyms

Latin letters

A,B,c,d	Coefficients of the Syamlal-O'Brien drag model (-)
c_t	Cuttings concentration threshold
A_c	Particle surface area (m^2)
A_s	Surface area of volume equivalent sphere (m^2)
C_D	Drag coefficient (-)
CMC	Carboxymethyl cellulose solution
CTV	Cuttings transport velocity
CTFV	Critical fluid transport velocity ($m.s^{-1}$)
DNS	Direct Numerical Simulations (-)
d_s	Volume equivalent particle diameter (m)
dP/dx	Pressure drop per unit length ($Pa.m^{-1}$)
e	Eccentricity (-)
e_{ss}	Coefficient of restitution (-)
ECD	Equivalent Circulating Density
F_r,n,p	Constants in the frictional pressure equation
$\vec{F}_{lift,s}$	Lift force (N)
$\vec{F}_s$	External body force (N)
$\vec{F}_{wl,s}$	Wall lubrication force (N)
$\vec{F}_{d,s}$	Turbulent dispersion force (N)

$\vec{F}_{lift,s}$ Lift force (N)
$\vec{F}_{vm,s}$ Virtual mass force (N)
$\vec{F}_{td,s}$ Turbulent dispersion force (N)
g Gravitational acceleration (m.s^{-2})
$g_{0,ss}$ Compressibility transition function (-)
I_{2D} Second variant of the deviatoric stress (-)
$\bar{\bar{I}}$ Unit tensor (-)
K_{sl} Interphase momentum exchange coefficient (-)
$K\acute{}_{sl}$ Modified interphase exchange coefficient (-)
K Consistency index (Pa.s^{n}).
LES Large Eddy Simulation
LWD Logging while drilling
$\dot{m}_{sl}$ Mass transfer from phase s to phase l (kg.s^{-1})
$\dot{m}_{ls}$ Mass transfer from phase l to phase s (kg.s^{-1})
n Flow behaviour index (-)
p Pressure (Pa)
p_s Solids pressure (Pa)
Q Flowrate
R_1 Radius of drillpipe (m)
R_2 Radius of wellbore (m)
ROP Rate of Penetration (ft.hr^{-1})
Re_s Particle Reynolds number (-)
S_q Source term (-)
τ_0 Yield Stress (N.m^{-2})
u_m Mean flow velocity (m.s^{-1})
$\vec{v}_{sl}$ Interphase velocity (m.s^{-1})
$\vec{v}_s$ Solid phase velocity (m.s^{-1})
$\vec{v}_l$ Liquid phase velocity (m.s^{-1})
$v_{r,s}$ Terminal velocity (m.s^{-1})
v_{slip} Cuttings slip velocity (m.s^{-1})
Y_p Yield point (Pa)

Greek letters
α_s Solid phase volume fraction (-)
$\alpha_{s,max}$ Solid volume fraction at maximum packing (-)
$\alpha_{s,min}$ Solid volume fraction after which friction occurs (-)
α_l Liquid phase volume fraction (-)
$\mu_{s,\,kin}$ Kinetic viscosity (Pa.s)
$\mu_{s,\,fr}$ Frictional viscosity (Pa.s)
λ_s Bulk viscosity (Pa.s)
λ_q Primary phase bulk viscosity (Pa.s)
μ_a Apparent viscosity (Pa.s)
μ_p Plastic viscosity (Pa.s)
μ_l Fluid viscosity (Pa.s)
μ_q Primary phase viscosity (Pa.s)
Θ_s Granular temperature (K)
ρ_s Solid phase density (kg.m^{-3})
$\rho_{r,s}$ Phase reference density (kg.m^{-3})
ρ_q Primary phase density (kg.m^{-3})
ρ_f Fluid density (kg.m^{-3})
$\hat{\rho}_q$ Effective phase density (kg.m^{-3})
β Hole inclination angle (degrees)
ψ Sphericity (-)
φ Cuttings bed porosity (%)
δ Offset distance (m)
ϕ Angle of internal friction (degrees)
ϕ_{ls} Energy exchange between fluid and solid phases (kg.m^{-1}s^{-3}))
η Drag modification factor

α_l Fluid phase volume fraction (-)
α_s Solid phase volume fraction (-)
τ Shear stress ($N.m^{-2}$)
$\bar{\bar{\tau}}_s$ Solid phase stress tensor (-)
γ Shear rate (s^{-1})
γ_{Θ_S} Collisional dissipation of energy ($kg.m^{-1}s^{-3}$)

8. References

Abu-Jdayil, B. and Ghannam, M., 2014. The modification of rheological properties of sodium bentonite-water dispersions with low viscosity CMC polymer effect. *Energy Sources, Part A: Recovery, Utilization, and Environmental Effects.* 36(10), 1037-1048.

Amanna, B. and Movaghar, M.R.K., 2016. Cuttings transport behavior in directional drilling using computational fluid dynamics (CFD). *Journal of Natural Gas Science and Engineering*, *34*, 670-679.

Akhshik, S., Behzad, M. and Rajabi, M., 2015. CFD–DEM approach to investigate the effect of drill pipe rotation on cuttings transport behavior. *J. Pet. Sci. Eng.* 127, 229-244.

Akhshik, S., Behzad, M. and Rajabi, M., 2016. CFD-DEM simulation of the hole cleaning process in a deviated well drilling: The effects of particle shape. *Particuology. 25*, 72-82.

Al-Kayiem, H.H., Zaki, N.M., Asyraf, M.Z., Elfeel, M.E., 2010. Simulation of the cuttings cleaning during the drilling operation. Am. J. Appl. Sci. 7 (6), 800–806

Byron, M.L., 2015. The rotation and translation of non-spherical particles in homogeneous isotropic turbulence. PhD Thesis, University of California, Berkeley, USA.

Busch, A., Islam, A., Martins, D.W., Iversen, F.P., Khatibi, M., Johansen, S.T., Time, R.W. and Meese, E.A., 2018. Cuttings-transport modeling–part 1: specification of benchmark parameters with a Norwegian-continental-shelf perspective. *SPE Drilling & Completion*.

Celigueta, M.A., Deshpande, K.M., Latorre, S. and Oñate, E., 2016. A FEM-DEM technique for studying the motion of particles in non-Newtonian fluids. Application to the transport of drill cuttings in wellbores. *Computational particle mechanics*, *3*(2), 263-276.

Chung, S.Y., Rhee, G.H. and Sung, H.J., 2002. Direct numerical simulation of turbulent concentric annular pipe flow: Part 1: Flow field. *International Journal of Heat and Fluid Flow*, *23*(4), 426-440.

Chung, S.Y. and Sung, H.J., 2005. Large-eddy simulation of turbulent flow in a concentric annulus with rotation of an inner cylinder. *International journal of heat and fluid flow*, *26*(2), 191-203.

Dalla Valle, J.M., 1943. Micromeritics the Technology of Fine Particles. Pitman Publishing Corporation. New York.

Duan, M., Miska, S.Z., Yu, M., Takach, N.E., Ahmed, R.M., Zettner, C.M., 2006. Transport of small cuttings in extended reach drilling. In: International Oil & Gas Conference and Exhibition in China. Society of Petroleum Engineers.

Eesa, M., Barigou, M., 2009. CFD investigation of the pipe transport of coarse solids in laminar power law fluids. *Chem. Eng. Sci.* 64 (2), 322–333.

Epelle, E.I. and Gerogiorgis, D.I., 2017a. A multiparametric CFD analysis of multiphase annular flows for oil and gas drilling applications. *Comput. Chem. Eng.*106, 645-661.

Epelle, E.I. and Gerogiorgis, D.I., 2018a. Transient and steady state analysis of drill cuttings transport phenomena under turbulent conditions. *Chemical Engineering Research and Design*, *131*, 520-544.

Epelle, E.I. and Gerogiorgis, D.I., 2018b. CFD modelling and simulation of drill cuttings transport efficiency in annular bends: effect of particle sphericity. *Journal of Petroleum Science and Engineering*, *170*, 992-1004.

Feiz, A.A., Ould-Rouis, M. and Lauriat, G., 2003. Large eddy simulation of turbulent flow in a rotating pipe. *International journal of heat and fluid flow*, *24*(3), 412-420.

Fluent, A. (2017). ANSYS Fluent theory guide 17.1. *Ansys Inc*, U.S.A.

Gidaspow, D., 1994. Multiphase flow and fluidization: continuum and kinetic theory descriptions. Academic press. NewYork.

Hakim, H., Katende, A., Sagala, F., Ismail, I. and Nsamba, H., 2018. Performance of polyethylene and polypropylene beads towards drill cuttings transportation in horizontal wellbore. *Journal of Petroleum Science and Engineering*, *165*, 962-969.

Heydari, O., Sahraei, E., & Skalle, P., 2017. Investigating the impact of drillpipe's rotation and eccentricity on cuttings transport phenomenon in various horizontal annuluses using computational fluid dynamics (CFD). *J. Pet. Sci. Eng*. 156, 801-813.

Hopkin, E.A., 1967. Factors affecting cuttings removal during rotary drilling. *Journal of Petroleum Technology*, 19(06), 807-814.

Hopkins, C.J. and Leicksenring, R.A., 1995, January. Reducing the risk of stuck pipe in the Netherlands. In *SPE/IADC Drilling Conference*. Society of Petroleum Engineers.

Johnson, P. C., & Jackson, R., 1987. Frictional–collisional constitutive relations for granular materials, with application to plane shearing. *J. Fluid Mech.* 176, 67-93.

Katende, A., Boyou, N.V., Ismail, I., Chung, D.Z., Sagala, F., Hussein, N. and Ismail, M.S., 2019. Improving the Performance of Oil Based Mud and Water Based Mud in a High Temperature Hole using Nanosilica Nanoparticles. *Colloids and Surfaces A: Physicochemical and Engineering Aspects*.

Kelin, W., Tie, Y., Xiaofeng, S., Shuai, S. and Shizhu, L., 2013. Review and analysis of cuttings transport in complex structural wells. *The Open Fuels & Energy Science Journal*, *6*(1).

Larsen, T.I., Pilehvari, A.A. and Azar, J.J., 1997. Development of a new cuttings-transport model for high angle wellbores including horizontal wells. *SPE Drilling & Completion*, *12*(02), 129-136.

Liu, N.S. and Lu, X.Y., 2005. Large eddy simulation of turbulent flows in a rotating concentric annular channel. *International journal of heat and fluid flow*, *26*(3), 378-392.

Lun, C., Savage, S., & Jeffrey, D., 1984. Kinetic theories for granular flow: inelastic particles in Couette flow and slightly inelastic particles in a general flowfield. *J. Fluid Mech*. 140, 223-256.

Mandø, M., Yin, C., Sørensen, H. and Rosendahl, L., 2007. On the modelling of motion of non-spherical particles in two-phase flow. In *6th Int. Conference Multiphase Flow. ICMF*, 9-13.

Manjula, E.V.P.J., Ariyaratne, W.H., Ratnayake, C. and Melaaen, M.C., 2017. A review of CFD modelling studies on pneumatic conveying and challenges in modelling offshore drill cuttings transport. *Powder Technology*, *305*, 782-793.

Massie, G.W., Castle-Smith, J., Lee, J.W. and Ramsey, M.S., 1995. Amocos training initiative reduces wellsite drilling problems. *Petroleum Engineer International*, *67*(3).

Mohammadzadeh, K., Hashemabadi, S.H. and Akbari, S., 2016. CFD simulation of viscosity modifier effect on cutting transport by oil based drilling fluid in wellbore. J. Nat. Gas Sci. Eng., 29, 355-364.

Moraveji, M.K., Sabah, M., Shahryari, A. and Ghaffarkhah, A., 2017. Investigation of drill pipe rotation effect on cutting transport with aerated mud using CFD approach. *Adv. Powder Technol.*, *28*(4), 1141-1153.

Naganawa, S., Sato, R. and Ishikawa, M., 2017. Cuttings-Transport Simulation Combined With Large-Scale-Flow-Loop Experimental Results and Logging-While-Drilling Data for Hole-Cleaning Evaluation in Directional Drilling. *SPE Drilling & Completion*, *32*(03), 194-207.

Nazari, T., Hareland, G. and Azar, J.J., 2010, January. Review of cuttings transport in directional well drilling: systematic approach. In *SPE Western Regional Meeting*. Society of Petroleum Engineers.

Ninokata, H., Okumura, T., Merzari, E. and Kano, T., 2005. Direct numerical simulation of turbulent flows in an eccentric annulus channel. *Annual Report of the Earth Simulator Center April*, *2006*.

Ofei, T., Irawan, S., & Pao, W., 2014. CFD method for predicting annular pressure losses and cuttings concentration in eccentric horizontal wells. *J. Pet. Eng.*

Pang, B., Wang, S., Wang, Q., Yang, K., Lu, H., Hassan, M. and Jiang, X., 2018a. Numerical prediction of cuttings transport behavior in well drilling using kinetic theory of granular flow. *Journal of Petroleum Science and Engineering*, *161*, 190-203.

Pang, B., Wang, S., Liu, G., Jiang, X., Lu, H. and Li, Z., 2018b. Numerical prediction of flow behavior of cuttings carried by Herschel-Bulkley fluids in horizontal well using kinetic theory of granular flow. *Powder Technology*, *329*, 386-398.

Rooki, R., Ardejani, F.D., Moradzadeh, A. and Norouzi, M., 2015. CFD Simulation of Rheological Model Effect on Cuttings Transport. *J. Dispersion Sci. Technol.* 36(3), 402-410.

Schaeffer, D., 1987. Instability in the evolution equations describing incompressible granular flow. *J. Diff. Eqns.* 66(1), 19-50.

Shah, M.T., Utikar, R.P., Pareek, V.K., Tade, M.O. and Evans, G.M., 2015. Effect of closure models on Eulerian–Eulerian gas–solid flow predictions in riser. *Powder Technology*, *269*, 247-258.

Sun, B., Xiang, H., Li, H. and Li, X., 2017. Modeling of the Critical Deposition Velocity of Cuttings in an Inclined-Slimhole Annulus. *SPE Journal*, *22*(04), 1213-1224.

Sobieski, W., 2009. Switch function and sphericity coefficient in the Gidaspow drag model for modeling solid-fluid systems. *Drying Technology*, *27*(2), 267-280.

Sorgun, M., 2010. Modeling of Newtonian Fluids and Cuttings Transport Analysis in High Inclination Wellbores with Pipe Rotation. Middle East Technical University, Turkey, Doctoral dissertation.

Syamlal, M. and O'Brien, T.J., 1987. The derivation of a drag coefficient formula from velocity-voidage correlations. *Technical Note, US Department of energy, Office of Fossil Energy, NETL, Morgantown, WV*.

Syamlal, M., Rogers, W. and O'Brien, T.J., 1993. MFIX documentation: Theory guide. *National Energy Technology Laboratory, Department of Energy, Technical Note DOE/METC-95/1013 and NTIS/DE95000031*.

Yeu, W.J., Katende, A., Sagala, F. and Ismail, I., 2019. Improving hole cleaning using low density polyethylene beads at different mud circulation rates in different hole angles. *Journal of Natural Gas Science and Engineering*, *61*, 333-343.

Yilmaz, D., 2012. Discrete Phase Simulations of Drilled Cuttings Transport Process in Highly Deviated Wells. Louisiana State University, USA, Master dissertation.

Yow, H.N., Pitt, M.J. and Salman, A.D., 2005. Drag correlations for particles of regular shape. *Adv. Powder Technol.* 16(4), 363-372.